Report

Current Biology

A Neofunctionalized X-Linked Ampliconic Gene Family Is Essential for Male Fertility and Equal Sex Ratio in Mice

Highlights

- *Slx* and *Slxl1* are mouse lineage-specific copies of their autosomal progenitor *Sycp3*
- *Slx* and *Slxl1* gene families are essential for male fertility
- Changes in *Slxl1* gene copy number distorts the ratio of male to female offspring
- *Slxl1* versus *Sly* competition for spindlin proteins may mediate sex-ratio distortion

Authors

Alyssa N. Kruger, Michele A. Brogley, Jamie L. Huizinga, Jeffrey M. Kidd, Dirk G. de Rooij, Yueh-Chiang Hu, Jacob L. Mueller

Correspondence

jacobmu@umich.edu

In Brief

A common assumption is that genes essential to a species survival must be deeply conserved. Kruger et al. report how two newly acquired X-linked gene families, *Slx* and *Slxl1*, evolved from an autosomal single-copy gene, massively duplicated, became essential for male fertility, and mediated the sex ratio of offspring by gene copy-number changes.

Kruger et al., 2019, Current Biology *29*, 3699–3706
November 4, 2019
https://doi.org/10.1016/j.cub.2019.08.057

CellPress

Current Biology
Report

A Neofunctionalized X-Linked Ampliconic Gene Family Is Essential for Male Fertility and Equal Sex Ratio in Mice

Alyssa N. Kruger,[1] Michele A. Brogley,[1] Jamie L. Huizinga,[1] Jeffrey M. Kidd,[1] Dirk G. de Rooij,[2,3] Yueh-Chiang Hu,[4,5] and Jacob L. Mueller[1,6,*]

[1]Department of Human Genetics, University of Michigan Medical School, 1241 E. Catherine Street, Ann Arbor, MI 48109, USA
[2]Reproductive Biology Group, Division of Developmental Biology, Department of Biology, Faculty of Science, Utrecht University, Padualaan 8, 3584 Utrecht, the Netherlands
[3]Center for Reproductive Medicine, Academic Medical Center, University of Amsterdam, Meibergdreef 9, 1105 AZ Amsterdam, the Netherlands
[4]Division of Developmental Biology, Cincinnati Children's Hospital Medical Center, 333 Burnet Avenue, Cincinnati, OH 45229, USA
[5]Department of Pediatrics, University of Cincinnati College of Medicine, 333 Burnet Avenue, Cincinnati, OH 45229, USA
[6]Lead Contact
*Correspondence: jacobmu@umich.edu
https://doi.org/10.1016/j.cub.2019.08.057

SUMMARY

The mammalian sex chromosomes harbor an abundance of newly acquired ampliconic genes, although their functions require elucidation [1–9]. Here, we demonstrate that the X-linked *Slx* and *Slxl1* ampliconic gene families represent mouse-specific neofunctionalized copies of a meiotic synaptonemal complex protein, *Sycp3*. In contrast to the meiotic role of *Sycp3*, CRISPR-loxP-mediated multi-megabase deletions of the *Slx* (5 Mb) and *Slxl1* (2.3Mb) ampliconic regions result in post-meiotic defects, abnormal sperm, and male infertility. Males carrying *Slxl1* deletions sire more male offspring, whereas males carrying *Slx* and *Slxl1* duplications sire more female offspring, which directly correlates with *Slxl1* gene dosage and gene expression levels. SLX and SLXL1 proteins interact with spindlin protein family members (SPIN1 and SSTY1/2) and males carrying *Slxl1* deletions downregulate a sex chromatin modifier, *Scml2*, leading us to speculate that *Slx* and *Slxl1* function in chromatin regulation. Our study demonstrates how newly acquired X-linked genes can rapidly evolve new and essential functions and how gene amplification can increase sex chromosome transmission.

RESULTS AND DISCUSSION

The megabase size and complexity of ampliconic (large [>10 kb] and nearly identical [>99% nucleotide identity] segmental duplications) regions have made it difficult to assess their evolutionary history and associated gene functions. Here, we examined the evolution and function of the *Slx* and *Slxl1* (*Sycp3*-like X-linked and *Slx*-like 1) ampliconic gene families in mice. The *Slx* and *Slxl1* gene families share sequence similarity with autosomal *Synaptonemal complex protein-3* (*Sycp3*), but the evolutionary history of *Slx* and *Slxl1* remains unclear [10, 11]. Double-knockdown studies of *Slx/Slxl1* exhibit post-meiotic spermatogenesis defects, male infertility, and meiotic drive [12, 13]. However, the lack of complete deletion mutants has hindered functional studies because *Slx/Slxl1* knockdowns are incomplete, may have off-target effects, are on a mixed genetic background, and do not allow one to assess the independent functions of *Slx* versus *Slxl1*. To more thoroughly characterize the functions of *Slx* and *Slxl1*, we generated precise, complete, and independent deletions of the megabase-sized *Slx* and *Slxl1* ampliconic regions on an inbred genetic background.

We first investigated the evolutionary history of *Slx* and *Slxl1*, by retracing *Slx* and *Slxl1* gene families' origination from *Sycp3*. Our sequence analyses indicate that in the mouse-rat ancestor, a single copy of *Sycp3* transposed via a copy and paste mechanism to an X-linked region syntenic to mouse *Slxl1. Slxl1* is thus the first family member to evolve, as no additional copies of *Slxl1*, *Slx*, or *Sly* are detectable on rat autosomal or Y chromosomal sequences (Figures 1A and S1A). In rat, *Slxl1* remains single-copy and appears non-functional, based upon low to no gene expression across tissues (Figures S1B and S1C). In mice, *Slxl1* maintains the intron-exon structure of *Sycp3* (Figure S2A), and a *Slxl1*-related gene family member, *Slx*, was acquired on an additional region of the mouse X chromosome (Figure 1A). *Slx* and *Slxl1* underwent repeated segmental duplications resulting in ~5Mb (*Slx*) and ~2.3 Mb (*Slxl1*) ampliconic regions, comprising 4% of the mouse X chromosome (Figures 1A and S3A) [1]. Mouse SLX and SLXL1 protein sequence is highly diverged from SYCP3 (<40% amino acid identity) (Figure S2B) and from rat SLXL1 (<39% amino acid identity) (Figure S1D), as compared to the median of all mouse-rat orthologs (95% amino acid identity) [16]. The high level of divergence suggests SLX/SLXL1 evolved new functions. Our findings establish the evolutionary acquisition and trajectory of the *Slx*, *Slxl1*, and *Sly* gene family, which was previously unclear.

The rapid sequence divergence of *Slx* and *Slxl1* from *Sycp3* appears to reflect neofunctionalization, based on their gene expression patterns and protein localization. SYCP3, a

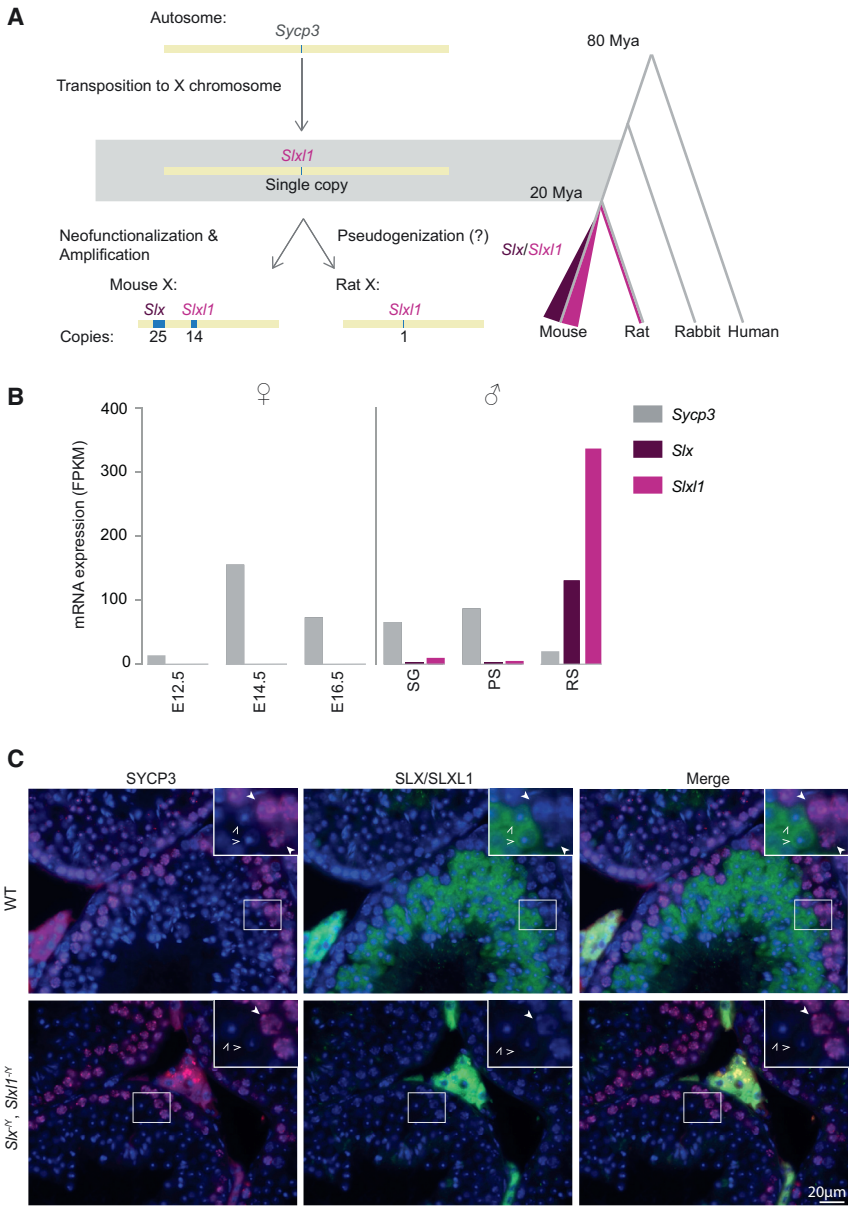

Figure 1. *Slx* and *Slxl1* Are Mouse-Lineage-Specific Neofunctionalized Copies of *Sycp3*

(A) *Sycp3* transposed to the X chromosome in the mouse-rat ancestor. Following mouse and rat speciation, *Slx* was acquired and both *Slx*/*Slxl1* were segmentally duplicated within the mouse lineage. *Sycp3* (light gray), *Slx* (purple), *Slxl1* (pink) are shown.

(B) mRNA-seq analysis on publically available datasets [14, 15]. In female mice, *Sycp3* expression is detected embryonically at E14.5 and in male mice, and *Sycp3* expression is detected in spermatogonia (SG) and pachytene spermatocytes (PS). *Slx* and *Slxl1* are expressed exclusively in the male germline, post-meiotically, in round spermatids (RS).

(C) Immunofluorescence of SYCP3 (red) and SLX/SLXL1 (green) on DAPI-stained testis histological sections from WT mice and mice lacking SLX/SLXL1 ($Slx^{-/Y}$, $Slxl1^{-/Y}$). RS (open arrow) and PS (closed arrow). Staining between tubules (Leydig cells) is non-specific.

See also Figures S1–S3.

component of the meiotic synaptonemal complex, is expressed in male and female meiotic germ cells and localizes to the nucleus (Figures 1B and 1C) [17]. In contrast, SLX and SLXL1 are expressed exclusively in post-meiotic testicular germ cells (Figures 1B and S3B) and are present within the cytoplasm (Figure 1C), supporting previous studies [18]. The cytoplasmic localization of SLX and SLXL1 is consistent with their loss of the putative nuclear localization signal and DNA-binding domain of SYCP3 (Figure S2B) [18–20]. Our findings suggest *Slx* and *Slxl1* are neofunctionalized copies of *Sycp3.*

To explore the independent functions of *Slx* and *Slxl1*, we used CRISPR and Cre/loxP (Figure 2B) to generate precise and complete multi-megabase deletions of *Slx* ($Slx^{-/Y}$) and *Slxl1* ($Slxl1^{-/Y}$). We generated individual deletions as they may have independent functions with 61% protein identity and having rapidly diverged from each other (dN/dS = 0.947) (Figures 2A–2C, S1D, S4A, and S4B). $Slx^{-/Y}$ and $Slxl1^{-/Y}$ mice exhibit wild-type (WT) fertility, fecundity, testis weights, sperm counts, and no observable spermatogenic defects via histology, which is in contrast to previous studies observing male fertility phenotypes in *Slx* knockdown mice (Figures 2D, S4C, and S4D) [12].

To test for genetic redundancy between *Slx* and *Slxl1*, we generated double deletions ($Slx^{-/Y}$, $Slxl1^{-/Y}$) via recombination of the independent deletions that are complete null mutants at the RNA and protein levels (Figures 1C, 2C, S4A, and S4B). In contrast to the independent deletions, double-deletion mice ($Slx^{-/Y}$, $Slxl1^{-/Y}$) are infertile and produce <1% the WT number of cauda epididymal sperm, which when present are morphologically severely abnormal (Figures 2D and 2F). Our double-deletion mice resemble previous knockdown studies, but the complete loss of *Slx* and *Slxl1* in $Slx^{-/Y}$, $Slxl1^{-/Y}$ mice now allows us to precisely identify that defects in post-meiotic germ cells occur during the transition from round spermatids to elongated spermatids at stage 7/8 (Figures 2E and S4F) [12]. The timing of elongation defects is consistent with our stage-specific determination of SLX/SLXL1 protein presence in WT males (Figures 1C and S4F). To assess whether $Slx^{-/Y}$, $Slxl1^{-/Y}$ mice produce competent meiotic products (round spermatids), we performed round spermatid injections (ROSI). Oocytes injected with round spermatids from WT or $Slx^{-/Y}$, $Slxl1^{-/Y}$ males develop to blastocysts at the same frequency (Figures S4G and S4B), indicating that $Slx^{-/Y}$, $Slxl1^{-/Y}$ round spermatids successfully progress through meiosis, supporting *Slx* and *Slxl1* being functionally distinct from meiotic *Sycp3* [21, 22]. To help explain why $Slx^{-/Y}$, $Slxl1^{-/Y}$ mice exhibit defects in spermatid elongation, we performed mRNA

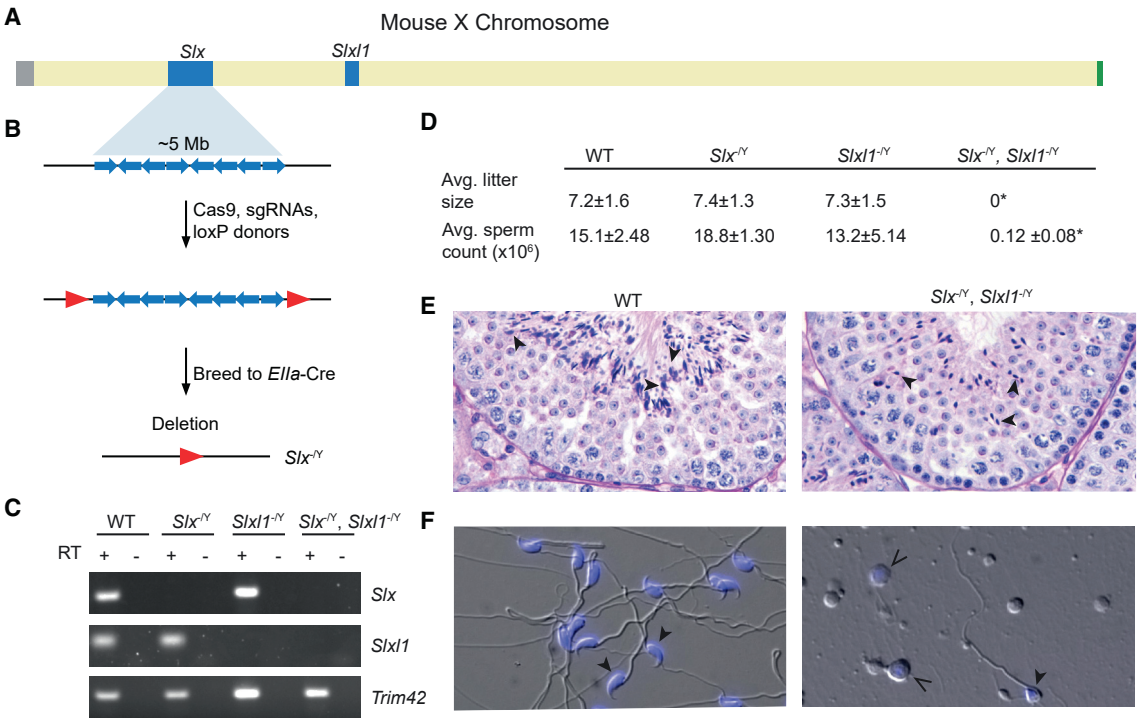

Figure 2. *Slx* and *Slxl1* Are Essential for Male Fertility and Exhibit Post-meiotic Spermatogenesis-Specific Defects

(A) Schematic representation of the mouse X chromosome. Ampliconic regions are shown in blue, centromere in gray, and pseudoautosomal region (PAR) in green.

(B) Schematic representation of *Slx* ampliconic region consisting of segmental duplications (blue arrows); red arrows denote loxP sites. Mice carrying loxP sites flanking the ampliconic region were mated to *Ella*-Cre carrying mice. *Slxl1*$^{-/Y}$ mice were generated in a complementary manner.

(C) RT-PCR (+) and no RT controls (–) performed on RNA isolated from adult testis. *Trim42* is a testis-specific gene that was used as a control. All primers are intron spanning.

(D) Average litter size and cauda epididymal sperm count including SD. Average litter size was determined by mating three males from each genotype against five females each for a total of 15 litters. Sperm were counted from at least three males. Two-tailed t tests were used to compare to WT, *$p < 0.0001$

(E) Periodic-acid Schiff-stained testis histology from WT and *Slx*$^{-/Y}$, *Slxl1*$^{-/Y}$ males. Stage 7 tubules and elongated spermatids (see black arrowheads) exhibit abnormal morphology in *Slx*$^{-/Y}$, *Slxl1*$^{-/Y}$ testis.

(F) Cauda epididymal sperm from a WT and *Slx*$^{-/Y}$, *Slxl1*$^{-/Y}$ male, DIC, and DAPI (closed arrows). Open arrows indicate cells that resemble round spermatids based upon DAPI stain present in *Slx*$^{-/Y}$, *Slxl1*$^{-/Y}$.

See also Figure S4.

sequencing (mRNA-seq) on round spermatids from *Slx*$^{-/Y}$, *Slxl1*$^{-/Y}$ and WT males and identified 990 misregulated genes (adjusted $p < 0.01$), which in combination likely perturb round spermatid elongation (Data S1). These results demonstrate that *Slx* and *Slxl1* acquired new functions in post-meiotic spermatids and function redundantly with each other [22].

While our results confirm that *Slx* and *Slxl1* are essential for male fertility, they do not explain their massive gene amplification (Figures S1B and S3A). The massive gene amplification of Slx and *Slxl1* has been proposed to be a result of their involvement in meiotic drive (the non-Mendelian inheritance of chromosomes); however, the importance of gene dosage has never been formally tested [3, 13]. If increases in gene dosage, via gene amplification, serve to increase chromosome transmission (meiotic drive), then complete deletions (*Slxl1*$^{-/Y}$ or *Slx*$^{-/Y}$) or duplications (*Slx*$^{Dup/Y}$ or *Slxl1*$^{Dup/Y}$ or *Slx*$^{Dup/Y}$, *Slxl1*$^{Dup/Y}$) (Figures 3A and 3B) of these regions should decrease or increase X chromosome transmission, respectively. *Slxl1*$^{-/Y}$ mice, but not *Slx*$^{-/Y}$ mice sire more male offspring (58.5% male, 141/241 pups) (two-tailed Fisher's exact test, $p < 0.05$) as compared to WT males (48.5% male, 94/194 pups; Figure 3C). Conversely, *Slx*$^{Dup/Y}$, *Slxl1*$^{Dup/Y}$ sire more female offspring (58.2% female, 181/311 pups; Figure 3C) as compared to WT (two-tailed Fisher's exact test, $p = 0.1672$) and is statistically significant when compared to *Slxl1*$^{-/Y}$ (two-tailed Fisher's exact test, $p < 0.0001$). We suspect differences between observing sex-ratio distortion in *Slx*$^{Dup/Y}$, *Slxl1*$^{Dup/Y}$ mice, but not in *Slxl1*$^{Dup/Y}$ mice, is due to unequal crossing over decreasing *Slxl1* copy number in the *Slxl1*$^{Dup/Y}$ line. Previous knockdown studies were unable to decipher the specific role of *Slxl1* and the impact of gene dosage in meiotic drive [12]. We suspect the distinct functions of *Slx* and *Slxl1* in meiotic drive are due to diverged residues (they share 61% amino acid identity) or gene expression levels, and the redundant functions in fertility are due to their conserved residues (Figure S2B). Our findings support the involvement of *Slxl1* in meiotic drive and via a gene dosage-dependent mechanism.

Slxl1 has been proposed to be in meiotic conflict, resulting in drive with a related Y-linked gene family *Sly* (*Sycp3*-like Y-linked), where *Sly* represses *Slx* and *Slxl1* gene expression

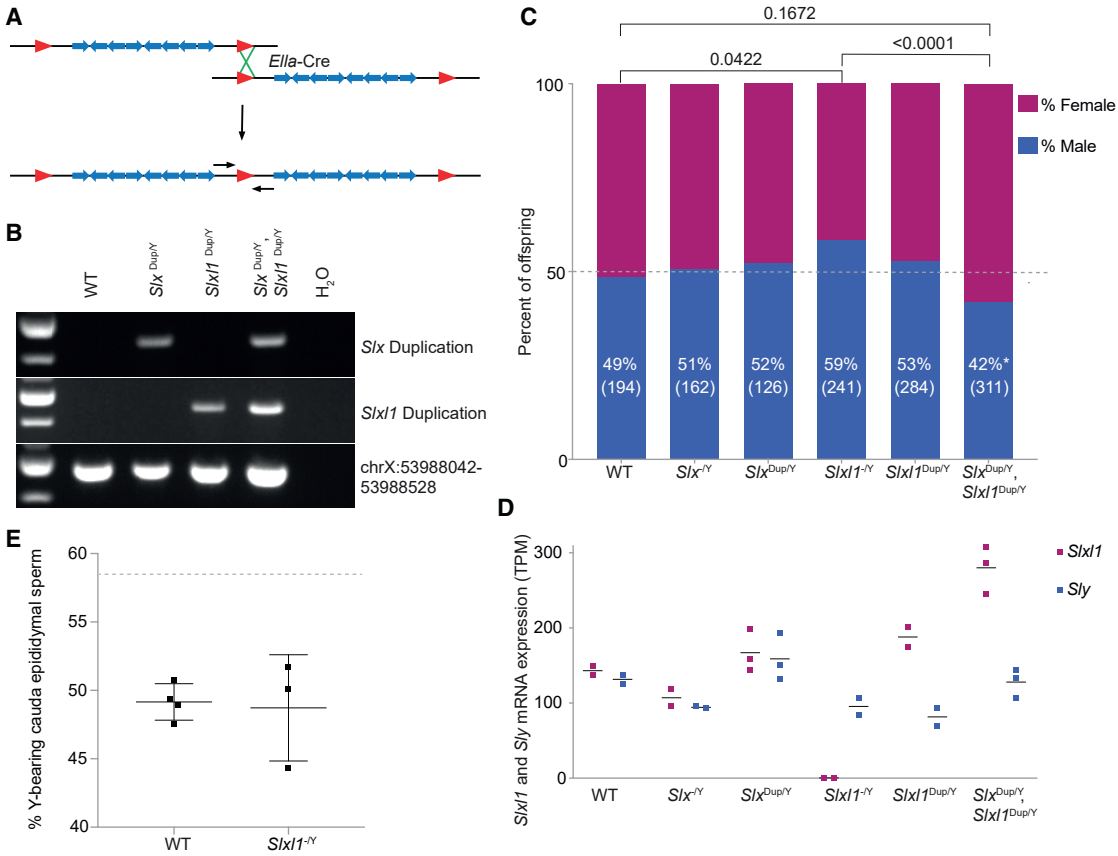

Figure 3. Changes in *Slxl1* Gene Dosage Results in Sex-Ratio Distortion of Offspring and *Slxl1* Gene Expression Levels

(A) Schematic representation of a floxed (red triangles) ampliconic region with segmental duplications (blue arrows). Duplications were generated by expression of *Ella*-Cre, and pups were genotyped using PCR primers spanning the duplication junction (small black arrows).

(B) Representative genotyping of WT, *Slx* duplication ($Slx^{Dup/Y}$), *Slxl1* duplication ($Slxl1^{Dup/Y}$), and *Slx*/*Slxl1* ($Slx^{Dup/Y}$ and $Slxl1^{Dup/Y}$) duplication mice. ChrX:53988042–53988528 is unique sequence, which controls for retaining the intervening sequence present between the *Slx* and *Slxl1* ampliconic regions.

(C) Males of each genotype were mated against WT females and progeny were sex genotyped. The percentage of male offspring is shown as a percentage along with the number of pups screened in parentheses. p values were calculated using a two-tailed Fisher's exact test, compared to experimental WT data (bars on top) and theoretical 50:50 data with an equivalent population size ($p < 0.05$, asterisk near male percentage).

(D) mRNA-seq was performed on isolated round spermatids. The horizontal line represents average expression across biological replicates (bullets) for *Slxl1* and *Sly*. TPM, transcripts per million.

(E) X and Y chromosome paint was performed on sperm collected from the cauda epididymis of WT and $Slxl1^{-/Y}$ males. Each bullet represents the percentage of Y-bearing sperm from one male, with overall mean and SD. The dotted line denotes expected percentage of Y-bearing sperm if ratio of X- to Y-bearing sperm reflected observed $Slxl1^{-/Y}$-sired offspring sex ratio. Differences between WT and $Slxl1^{-/Y}$ are not significant; Fisher's exact test was two-tailed.

See also Data S1.

[13, 23]. Our finding that *Slxl1* gene dosage contributes to meiotic drive (Figure 3C) led us to test whether mice with sex-ratio distortion exhibit corresponding gene expression changes in *Sly*, *Slxl1*, or both. We performed mRNA-seq on round spermatids and found that increases in *Slxl1* gene dosage have corresponding increases in *Slxl1* expression, while *Sly* expression remains relatively unchanged (Figure 3D). Our findings suggest the ratio of *Slxl1* to *Sly* gene expression levels mediates meiotic drive (Figure 3D); however, the ratio does not affect the number of X- versus Y-bearing sperm from $Slxl1^{-/Y}$ mice (Figure 3E). Meiotic drive likely impacts the relative fitness of X- versus Y-bearing sperm via changes in SLXL1 to SLY protein abundance and interactions with protein partners.

We next identified SLX- and SLXL1-interacting proteins that may contribute to meiotic drive. We performed endogenous SLX/SLXL1 co-immunoprecipitation and mass spectrometry on testis lysates from WT, $Slx^{-/Y}$, $Slxl1^{-/Y}$ and $Slx^{-/Y}$, $Slxl1^{-/Y}$ mice. Candidates were prioritized by their reproducibility across multiple WT samples and absence in $Slx^{-/Y}$, $Slxl1^{-/Y}$ samples. We identified spindlin family members SPIN1, SSTY1 and SSTY2 (SSTY1/2), and 26S proteasome components PSMC1 and PSMD4 (Figure 4A; Table S1). We did not immunoprecipitate SLY, suggesting SLXL1 and SLY conflict does not occur through direct protein interactions. Instead, SLX, SLXL1, and SLY may compete for spindlin family members, as SSTY1/2 have been shown to interact with SLX, SLXL1, and SLY [24]. SLX and SLXL1 are present in all haploid spermatids (Figure 1C) and

A

SLX/SLXL1 IP Mass Spec PSMs

Gene	WT	*Slx* $^{-/Y}$	*Slxl1* $^{-/Y}$	*Slx* $^{-/Y}$, *Slxl1* $^{-/Y}$
SLX*	121	0	93	0
SLXL1	87	73	0	0
SPIN1	15	13	10	0
SSTY2	11	4	7	0
PSMC1	7	5	3	0
SSTY1	6	0	3	0
PSMD4	6	4	4	0

B

	Adjusted p-values					
Scml2	0.99	0.99	0.001	0.86	0.99	0.90
WT vs.	*Slx* $^{-/Y}$	*Slx* $^{Dup/Y}$	*Slxl1* $^{-/Y}$	*Slxl1* $^{Dup/Y}$	*Slx* $^{Dup/Y}$, *Slxl1* $^{Dup/Y}$	*Slx* $^{-/Y}$, *Slxl1* $^{-/Y}$

C

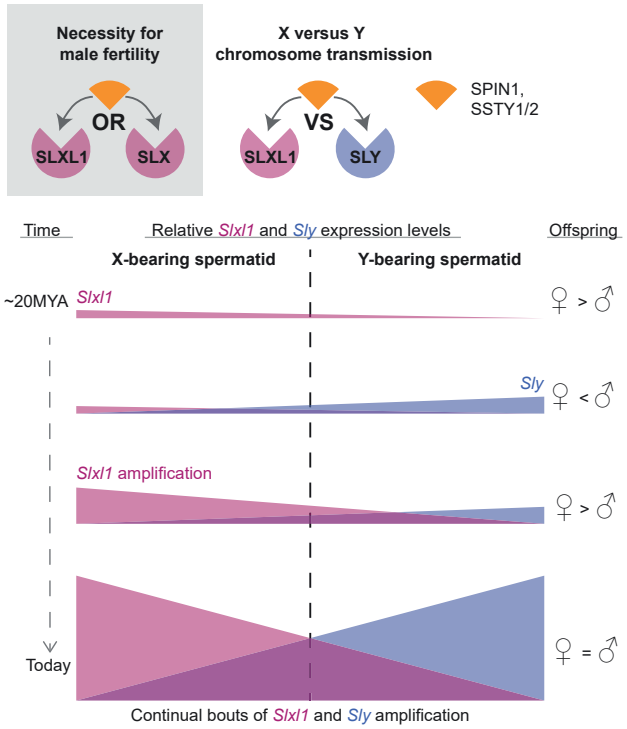

Figure 4. SLX/SLXL1 Interact with Spindlin Family Members and Regulate Chromatin

(A) Mass spectrometry results from SLX/SLXL1 immunoprecipitations on WT, *Slx*$^{-/Y}$, *Slxl1*$^{-/Y}$, and *Slx*$^{-/Y}$, *Slxl1*$^{-/Y}$ whole-testis lysates. PSMs (peptide-to-spectrum matches) were quantified to determine relative protein abundance. Candidates were filtered by high confidence (<1% false discovery rate [FDR]) and reproducibility. (*additional SLX accessions were removed for simplicity; see Table S1 for biological replicates.)

(B) Expression level adjusted p values for *Scml2* isoform NM_001290652 when comparing WT versus deletion or duplication genotype round spermatid mRNA-seq samples.

(C) We speculate SLX or SLXL1 interactions with spindlin family members SPIN1 and SSTY1/2 are essential for fertility and SLXL1 and SLY competition for SPIN1 and SSTY1/2 influences chromosome transmission through the sharing of proteins and transcripts across cytoplasmic bridges. Changes in the relative expression of *Slxl1* to *Sly* result in corresponding changes in the fitness of X and Y sperm that influence offspring sex ratio.

therefore could compete with SLY for SPIN1 and SSTY1/2 by diffusing across cytoplasmic bridges connecting haploid spermatids (Figure 4C). SPIN1 is a chromatin reader and post-transcriptional regulator of mRNA stability [25, 26]. SPIN1 binds H3K4me3-R8me2a via its Spin/Ssty domains, which are shared with SSTY1/2 [26]. We hypothesize that changes in SLXL1 to SLY abundance could alter SPIN1 distribution and may have transcriptomic consequences that impact the downstream fitness of X- versus Y-bearing sperm. PSMC1 and PSMD4 may be non-specific interactions, as our antibody has non-specific localization to the acrosome (present in *Slx*$^{-/Y}$, *Slxl1*$^{-/Y}$) where proteases are known to reside (Figure S4E).

Based on SLXL1 and SLY protein interaction with spindlin family members SPIN1 and SSTY1/2, we speculated that misregulated X- or Y-linked genes may cause X- versus Y-sperm fitness differences. Comparison of round spermatid mRNA-seq data from WT versus *Slxl1*$^{-/Y}$ males identified five X-linked (not including *Slxl1* gene family members), two Y-linked and 50 autosomal genes that are significantly misregulated (adjusted $p < 0.01$) (Data S1). One of the seven is an alternative splice form of *Scml2* that is significantly downregulated only in *Slxl1*$^{-/Y}$ males (Figure 4B; Data S1). SCML2 is a germline-specific polycomb group protein that regulates sex chromosome-wide silencing in meiotic and post-meiotic cells via chromatin modifications [27]. Together, the interactions of SLXL1 with SPIN1 and SSTY1/2, and the downregulation of *Scml2,* lead us to speculate that changes in round spermatid chromatin may mediate meiotic drive.

The neofunctionalization and amplification of *Slx* and *Slxl1* evolved in the past ~20 MY of mouse-lineage evolution, creating a gene family that functions in a post-meiotic manner that is essential for male fertility (Figure 4C). Our findings build upon previous studies, providing new insights into the evolution, neofunctionalization, and independent contributions of *Slx* versus *Slxl1* [12, 13]. Additionally, we demonstrate the impact gene dosage has on gene expression and conflict between *Slxl1* and *Sly*. We propose that the acquisition of *Slxl1* in the rat-mouse ancestor conferred a selective advantage to increase X chromosome transmission (Figure 4C). In response, *Sly* evolved on the Y chromosome specifically in the mouse lineage to equalize the sex ratio. The rapid changes in gene dosage, gene expression levels, and protein sequence chronicle the continued bouts of *Slx/Slxl1* versus *Sly* genetic conflict within the mouse lineage (Figure 4C). In the present day C57BL/6J mouse strain, *Slxl1* is likely a primary mediator of meiotic drive, because the frequency of female offspring correlates with increases (*Slx*$^{Dup/Y}$, *Slxl1*$^{Dup/Y}$)

and decreases ($Slxl1^{-/Y}$) in *Slxl1* gene dosage (Figures 3C and 3D). These evolutionary signatures inform our proposed model in which SLXL1 and SLY compete for interactions with spindlin family members SPIN1 and SSTY1/2 in a dose-dependent manner (Figure 4C). We speculate the interaction of SLX/SLXL1 with the conserved and ubiquitously expressed SPIN1 mediates male fertility, and SLX/SLXL1 interaction with the newly acquired and ampliconic Y-linked gene family SSTY1/2 mediates meiotic drive (Figure 4C) [3, 28]. Consistent with this idea, the chromatin reader SSTY1/2 localizes to X and Y chromatin, where it can have impacts on the localization and regulation of transcription [24].

Mammalian sex chromosomes harbor a plethora of newly acquired ampliconic genes expressed predominantly in the testis [1–6]. Is X-Y co-amplification of newly acquired genes a universal phenomenon continually reshaping sex chromosome evolution? In mice, *Ssty1/2* and *Sstx* are X-Y co-amplified gene families that pre-date *Slx*, *Slxl1*, and *Sly* [3, 10]. *Ssty1/2* and *Sstx* may represent a former or current system of genetic conflict. Given SLX, SLXL1, and SLY proteins interact with SSTY1/2, it is tempting to speculate that conflict between gene families on the X and Y chromosome can continuously re-emerge and converge upon pre-existing pathways. The sex chromosomes are a known battleground for genes in conflict, and competition between co-amplified X- and Y-linked genes could provide the genetic basis for speciation and hybrid male sterility; both processes are known to be associated with the X chromosome [29–31]. Indeed, in other mammals there are hints of entirely new co-amplified X-Y gene families [32]. More complete assemblies of X and Y chromosomes will determine the extent of X-Y gene co-amplification across mammals. We conclude that prime candidates of X-Y genetic conflict can be readily identified in future studies by the presence of three defining signatures: new acquisition, X-Y co-amplification, and rapid sequence evolution.

STAR★METHODS

Detailed methods are provided in the online version of this paper and include the following:

- KEY RESOURCES TABLE
- LEAD CONTACT AND MATERIALS AVAILABILITY
- EXPERIMENTAL MODEL AND SUBJECT DETAILS
- METHOD DETAILS
  - Gene expression of mouse and rat X/Y co-amplified genes
  - Round spermatid FACS isolation and library generation
  - Generation of transgenic lines
  - Testis Histology
  - Immunohistochemistry
  - RT-PCR
  - Assaying Fertility
  - X-Y Chromosome Paint
  - Co-Immunoprecipitation and Mass Spectrometry
  - Estimation of amplicon copy number
  - Comparisons of exon-intron structure
  - Dot-plots
  - Round spermatid Injections (ROSI)
- QUANTIFICATION AND STATISTICAL ANALYSIS
- DATA AND CODE AVAILABILITY

SUPPLEMENTAL INFORMATION

Supplemental Information can be found online at https://doi.org/10.1016/j.cub.2019.08.057.

ACKNOWLEDGMENTS

We acknowledge Cincinnati Children's Hospital Medical Center Transgenic Animal and Genome Editing Core for mutant mouse production, Celvie Yuan and Yang Yu for their assistance with ROSI experiments, the University of Michigan Flow Cytometry Shared Resource Laboratory for FACS, DNA Sequencing Core for Sanger, Next Generation Sequencing, Venkatesha Basrur at the Proteomics Resource facility for mass spectrometry, and Cancer Center Tissue Core for generating testis histological sections. We thank D. Ginsburg for sharing *Ella*-Cre mice. We thank M. Arlt, S. Kalantry, J. Moran, C. Swanepoel, and Y. Yamashita for their comments. This work was supported by NIH grants HD064753 and HD094736 to J.L.M. and T32GM007544 to A.N.K. and a National Science Foundation Graduate Research Fellowship DGE 1256260 to A.N.K.

AUTHOR CONTRIBUTIONS

A.N.K. and J.L.M. planned the project. A.N.K., M.A.B., and J.L.H. performed experiments. D.G.D. performed histological characterization. J.M.K. performed copy-number estimates. A.N.K. and J.L.M. wrote the manuscript.

DECLARATION OF INTERESTS

The authors declare no competing interests.

Received: June 18, 2019
Revised: July 25, 2019
Accepted: August 21, 2019
Published: October 17, 2019

REFERENCES

1. Mueller, J.L., Mahadevaiah, S.K., Park, P.J., Warburton, P.E., Page, D.C., and Turner, J.M. (2008). The mouse X chromosome is enriched for multicopy testis genes showing postmeiotic expression. Nat. Genet. *40*, 794–799.
2. Mueller, J.L., Skaletsky, H., Brown, L.G., Zaghlul, S., Rock, S., Graves, T., Auger, K., Warren, W.C., Wilson, R.K., and Page, D.C. (2013). Independent specialization of the human and mouse X chromosomes for the male germ line. Nat. Genet. *45*, 1083–1087.
3. Soh, Y.Q., Alföldi, J., Pyntikova, T., Brown, L.G., Graves, T., Minx, P.J., Fulton, R.S., Kremitzki, C., Koutseva, N., Mueller, J.L., et al. (2014). Sequencing the mouse Y chromosome reveals convergent gene acquisition and amplification on both sex chromosomes. Cell *159*, 800–813.
4. Skaletsky, H., Kuroda-Kawaguchi, T., Minx, P.J., Cordum, H.S., Hillier, L., Brown, L.G., Repping, S., Pyntikova, T., Ali, J., Bieri, T., et al. (2003). The male-specific region of the human Y chromosome is a mosaic of discrete sequence classes. Nature *423*, 825–837.
5. Hughes, J.F., Skaletsky, H., Pyntikova, T., Graves, T.A., van Daalen, S.K., Minx, P.J., Fulton, R.S., McGrath, S.D., Locke, D.P., Friedman, C., et al. (2010). Chimpanzee and human Y chromosomes are remarkably divergent in structure and gene content. Nature *463*, 536–539.
6. Murphy, W.J., Pearks Wilkerson, A.J., Raudsepp, T., Agarwala, R., Schäffer, A.A., Stanyon, R., and Chowdhary, B.P. (2006). Novel gene acquisition on carnivore Y chromosomes. PLoS Genet. *2*, e43.
7. Janečka, J.E., Davis, B.W., Ghosh, S., Paria, N., Das, P.J., Orlando, L., Schubert, M., Nielsen, M.K., Stout, T.A.E., Brashear, W., et al. (2018).

Horse Y chromosome assembly displays unique evolutionary features and putative stallion fertility genes. Nat. Commun. *9*, 2945.

8. Skinner, B.M., Sargent, C.A., Churcher, C., Hunt, T., Herrero, J., Loveland, J.E., Dunn, M., Louzada, S., Fu, B., Chow, W., et al. (2016). The pig X and Y chromosomes: structure, sequence, and evolution. Genome Res. *26*, 130–139.
9. Kuroda-Kawaguchi, T., Skaletsky, H., Brown, L.G., Minx, P.J., Cordum, H.S., Waterston, R.H., Wilson, R.K., Silber, S., Oates, R., Rozen, S., and Page, D.C. (2001). The AZFc region of the Y chromosome features massive palindromes and uniform recurrent deletions in infertile men. Nat. Genet. *29*, 279–286.
10. Ellis, P.J., Bacon, J., and Affara, N.A. (2011). Association of Sly with sex-linked gene amplification during mouse evolution: a side effect of genomic conflict in spermatids? Hum. Mol. Genet. *20*, 3010–3021.
11. Touré, A., Clemente, E.J., Ellis, P., Mahadevaiah, S.K., Ojarikre, O.A., Ball, P.A., Reynard, L., Loveland, K.L., Burgoyne, P.S., and Affara, N.A. (2005). Identification of novel Y chromosome encoded transcripts by testis transcriptome analysis of mice with deletions of the Y chromosome long arm. Genome Biol. *6*, R102.
12. Cocquet, J., Ellis, P.J., Yamauchi, Y., Riel, J.M., Karacs, T.P., Rattigan, A., Ojarikre, O.A., Affara, N.A., Ward, M.A., and Burgoyne, P.S. (2010). Deficiency in the multicopy Sycp3-like X-linked genes Slx and Slxl1 causes major defects in spermatid differentiation. Mol. Biol. Cell *21*, 3497–3505.
13. Cocquet, J., Ellis, P.J., Mahadevaiah, S.K., Affara, N.A., Vaiman, D., and Burgoyne, P.S. (2012). A genetic basis for a postmeiotic X versus Y chromosome intragenomic conflict in the mouse. PLoS Genet. *8*, e1002900.
14. Hammoud, S.S., Low, D.H., Yi, C., Carrell, D.T., Guccione, E., and Cairns, B.R. (2014). Chromatin and transcription transitions of mammalian adult germline stem cells and spermatogenesis. Cell Stem Cell *15*, 239–253.
15. Soh, Y.Q., Junker, J.P., Gill, M.E., Mueller, J.L., van Oudenaarden, A., and Page, D.C. (2015). A gene regulatory program for meiotic prophase in the fetal ovary. PLoS Genet. *11*, e1005531.
16. Gibbs, R.A., Weinstock, G.M., Metzker, M.L., Muzny, D.M., Sodergren, E.J., Scherer, S., Scott, G., Steffen, D., Worley, K.C., Burch, P.E., et al.; Rat Genome Sequencing Project Consortium (2004). Genome sequence of the Brown Norway rat yields insights into mammalian evolution. Nature *428*, 493–521.
17. Page, S.L., and Hawley, R.S. (2004). The genetics and molecular biology of the synaptonemal complex. Annu. Rev. Cell Dev. Biol. *20*, 525–558.
18. Reynard, L.N., Turner, J.M., Cocquet, J., Mahadevaiah, S.K., Touré, A., Höög, C., and Burgoyne, P.S. (2007). Expression analysis of the mouse multi-copy X-linked gene Xlr-related, meiosis-regulated (Xmr), reveals that Xmr encodes a spermatid-expressed cytoplasmic protein, SLX/XMR. Biol. Reprod. *77*, 329–335.
19. Baier, A., Alsheimer, M., Volff, J.N., and Benavente, R. (2007). Synaptonemal complex protein SYCP3 of the rat: evolutionarily conserved domains and the assembly of higher order structures. Sex Dev. *1*, 161–168.
20. Syrjänen, J.L., Pellegrini, L., and Davies, O.R. (2014). A molecular model for the role of SYCP3 in meiotic chromosome organisation. eLife *3*. Published online June 20, 2014. https://doi.org/10.7554/eLife.02963.
21. Sato, T., Katagiri, K., Yokonishi, T., Kubota, Y., Inoue, K., Ogonuki, N., Matoba, S., Ogura, A., and Ogawa, T. (2011). In vitro production of fertile sperm from murine spermatogonial stem cell lines. Nat. Commun. *2*, 472.
22. Yuan, L., Liu, J.G., Zhao, J., Brundell, E., Daneholt, B., and Höög, C. (2000). The murine SCP3 gene is required for synaptonemal complex assembly, chromosome synapsis, and male fertility. Mol. Cell *5*, 73–83.
23. Cocquet, J., Ellis, P.J., Yamauchi, Y., Mahadevaiah, S.K., Affara, N.A., Ward, M.A., and Burgoyne, P.S. (2009). The multicopy gene Sly represses the sex chromosomes in the male mouse germline after meiosis. PLoS Biol. *7*, e1000244.
24. Comptour, A., Moretti, C., Serrentino, M.E., Auer, J., Ialy-Radio, C., Ward, M.A., Touré, A., Vaiman, D., and Cocquet, J. (2014). SSTY proteins co-localize with the post-meiotic sex chromatin and interact with regulators of its expression. FEBS J. *281*, 1571–1584.
25. Chew, T.G., Peaston, A., Lim, A.K., Lorthongpanich, C., Knowles, B.B., and Solter, D. (2013). A tudor domain protein SPINDLIN1 interacts with the mRNA-binding protein SERBP1 and is involved in mouse oocyte meiotic resumption. PLoS ONE *8*, e69764.
26. Su, X., Zhu, G., Ding, X., Lee, S.Y., Dou, Y., Zhu, B., Wu, W., and Li, H. (2014). Molecular basis underlying histone H3 lysine-arginine methylation pattern readout by Spin/Ssty repeats of Spindlin1. Genes Dev. *28*, 622–636.
27. Adams, S.R., Maezawa, S., Alavattam, K.G., Abe, H., Sakashita, A., Shroder, M., Broering, T.J., Sroga Rios, J., Thomas, M.A., Lin, X., et al. (2018). RNF8 and SCML2 cooperate to regulate ubiquitination and H3K27 acetylation for escape gene activation on the sex chromosomes. PLoS Genet. *14*, e1007233.
28. Staub, E., Mennerich, D., and Rosenthal, A. (2002). The Spin/Ssty repeat: a new motif identified in proteins involved in vertebrate development from gamete to embryo. Genome Biol. *3*, research0003.
29. Presgraves, D.C. (2008). Sex chromosomes and speciation in Drosophila. Trends Genet. *24*, 336–343.
30. Forejt, J. (1996). Hybrid sterility in the mouse. Trends Genet. *12*, 412–417.
31. Zanders, S.E., and Unckless, R.L. (2019). Fertility costs of meiotic drivers. Curr. Biol. *29*, R512–R520.
32. Larson, E.L., Kopania, E.E.K., and Good, J.M. (2018). Spermatogenesis and the evolution of mammalian sex chromosomes. Trends Genet. *34*, 722–732.
33. Bray, N.L., Pimentel, H., Melsted, P., and Pachter, L. (2016). Near-optimal probabilistic RNA-seq quantification. Nat. Biotechnol. *34*, 525–527.
34. Love, M.I., Huber, W., and Anders, S. (2014). Moderated estimation of fold change and dispersion for RNA-seq data with DESeq2. Genome Biol. *15*, 550.
35. Haeussler, M., Schönig, K., Eckert, H., Eschstruth, A., Mianné, J., Renaud, J.B., Schneider-Maunoury, S., Shkumatava, A., Teboul, L., Kent, J., et al. (2016). Evaluation of off-target and on-target scoring algorithms and integration into the guide RNA selection tool CRISPOR. Genome Biol. *17*, 148.
36. Hach, F., Hormozdiari, F., Alkan, C., Hormozdiari, F., Birol, I., Eichler, E.E., and Sahinalp, S.C. (2010). mrsFAST: a cache-oblivious algorithm for short-read mapping. Nat. Methods *7*, 576–577.
37. Pendleton, A.L., Shen, F., Taravella, A.M., Emery, S., Veeramah, K.R., Boyko, A.R., and Kidd, J.M. (2018). Comparison of village dog and wolf genomes highlights the role of the neural crest in dog domestication. BMC Biol. *16*, 64.
38. Pavesi, G., Zambelli, F., Caggese, C., and Pesole, G. (2008). Exalign: a new method for comparative analysis of exon-intron gene structures. Nucleic Acids Res. *36*, e47.
39. Merkin, J., Russell, C., Chen, P., and Burge, C.B. (2012). Evolutionary dynamics of gene and isoform regulation in mammalian tissues. Science *338*, 1593–1599.
40. Necsulea, A., and Kaessmann, H. (2014). Evolutionary dynamics of coding and non-coding transcriptomes. Nat. Rev. Genet. *15*, 734–748.
41. Chalmel, F., Lardenois, A., Evrard, B., Rolland, A.D., Sallou, O., Dumargne, M.C., Coiffec, I., Collin, O., Primig, M., and Jégou, B. (2014). High-resolution profiling of novel transcribed regions during rat spermatogenesis. Biol. Reprod. *91*, 5.
42. Gaysinskaya, V., Soh, I.Y., van der Heijden, G.W., and Bortvin, A. (2014). Optimized flow cytometry isolation of murine spermatocytes. Cytometry A *85*, 556–565.
43. Scott, M.A., and Hu, Y.C. (2019). Generation of CRISPR-edited rodents using a Piezo-driven zygote injection technique. Methods Mol. Biol. *1874*, 169–178.
44. Ahmed, E.A., and de Rooij, D.G. (2009). Staging of mouse seminiferous tubule cross-sections. Methods Mol. Biol. *558*, 263–277.

45. Perez-Riverol, Y., Csordas, A., Bai, J., Bernal-Llinares, M., Hewapathirana, S., Kundu, D.J., Inuganti, A., Griss, J., Mayer, G., Eisenacher, M., et al. (2019). The PRIDE database and related tools and resources in 2019: improving support for quantification data. Nucleic Acids Res. *47* (D1), D442–D450.

46. Guryev, V., Saar, K., Adamovic, T., Verheul, M., van Heesch, S.A., Cook, S., Pravenec, M., Aitman, T., Jacob, H., Shull, J.D., et al. (2008). Distribution and functional impact of DNA copy number variation in the rat. Nat. Genet. *40*, 538–545.

47. Cortez, D., Marin, R., Toledo-Flores, D., Froidevaux, L., Liechti, A., Waters, P.D., Grützner, F., and Kaessmann, H. (2014). Origins and functional evolution of Y chromosomes across mammals. Nature *508*, 488–493.

48. Ogura, A., Matsuda, J., Asano, T., Suzuki, O., and Yanagimachi, R. (1996). Mouse oocytes injected with cryopreserved round spermatids can develop into normal offspring. J. Assist. Reprod. Genet. *13*, 431–434.

49. Kishigami, S., and Wakayama, T. (2007). Efficient strontium-induced activation of mouse oocytes in standard culture media by chelating calcium. J. Reprod. Dev. *53*, 1207–1215.

STAR★METHODS

KEY RESOURCES TABLE

REAGENT or RESOURCE	SOURCE	IDENTIFIER
Antibodies		
Anti-SLX/SLXL1, Rabbit polyclonal	This manuscript	N/A
Anti-SCP3, mouse monoclonal	Abcam	Cat# ab97672; RRID: AB_10678841 Lot#GR149989-1
Peroxidase AffiniPure Donkey Anti-Rabbit IgG	Jackson ImmunoResearch	Cat# 711-035-152; RRID: AB_10015282 Lot#117685
FITC AffiniPure Donkey Anti-Rabbit IgG (H+L)	Jackson ImmunoResearch	Cat# 711-095-152; RRID: AB_2315776 Lot# 114194
Rhodamine RedX AffiniPure Donkey Anti-Mouse IgG (H+L)	Jackson ImmunoResearch	Cat# 715-295-151; RRID: AB_2340832 Lot#116974
Chemicals, Peptides, and Recombinant Proteins		
Collagenase type I	Worthington Biochemical Corporation	Cat# LS004196
DNase I	Worthington Biochemical Corporation	Cat# LS002138
Trypsin	Life Technologies	Cat# 15090-046
Hoechst 33342	Setareh Biotech	Cat# 7026
Propidium iodide	Acros Organics	Cat# 440300250
TRIzol LS	Thermo Fisher Scientific	Cat# 10296010
Agencourt AMPure XP	Beckman Coulter	Cat# A63881
Viagen DirectPCR lysis reagent	Viagen Biotech	Cat# 102-T
Bouin's Fixative	RICCA Chemical Company	Cat# 1120-32
Schiff's Reagent	Sigma-Aldrich	Cat# 3952016
Hematoxylin Solution	Sigma-Aldrich	Cat# MHS16
Trizol	LifeTechnologies	Cat# 15596026
Superscript II	Invitrogen	Cat# 18064071
Dithiothreitol (DTT)	Fisher Scientific	Cat# BP172-5
Triton X	Sigma-Aldrich	Cat# X100
Formamide deionized	Bio Basic	Cat# 75-12-7
XMP X Green XCyting Mouse Chromosome Paint and XMP Y Orange XCyting Mouse Chromosome Paint	MetaSystems Probes	Cat# D-1420-050-FI, D-1421-050-OR
VECTASHIELD with DAPI	Vector Laboratories	Cat# H-1200
protein A Dynabeads	Life Technologies	Cat# 10002D
cOmplete, Mini, EDTA-free Protease Inhibitor Cocktail	Sigma Aldrich	Cat# 11836170001
blood cell lysis solution	Miltenyi Biotec	Cat# 130-094-183
Pronase E	SERVA	Cat# 11478622
Paraformaldehyde 16%	Electron Microscopy Sciences	Cat# 15710
Nonidet-P40 Substitute	US Biological	Cat# N3500
Critical Commercial Assays		
RNeasy Mini Kit and RNase-Free DNase Set	QIAGEN	Cat# 74104, 79254
NEBNext Ultra II Directional RNA Library Prep Kit	NEB	Cat# E7760
MEGAshorscript T7 kit	ThermoFisher	Cat# AM1354
mMESSAGE mMACHINE T7 ULTRA kit	ThermoFisher	Cat# AM1345
MEGAclear Kit	ThermoFisher	Cat# AM1908
Turbo DNase	Life Technologies	Cat# AM1907

(*Continued on next page*)

Continued		
REAGENT or RESOURCE	SOURCE	IDENTIFIER
Deposited Data		
Mouse Testis Immunoprecipitation- SLX/SLXL1	ProteomeXchange Consortium, PRIDE	PXD014276
Genome resequencing for a Rattus norvegicus (rat) female individual	SRA	SRP029216
Mouse tissue panel mRNA-seq	SRA	SRP016501
Mouse fetal ovary mRNA-seq	SRA	SRP058992
Mouse adult ovary mRNA-seq	SRA	SRP017959
Mouse sorted testicular germ cells mRNA-seq	SRA	SRP113417
Rat sorted testicular germ cells mRNA-seq	SRA	SRP026340
Mouse sorted testicular germ cells mRNA-seq	SRA	SRP200106
Experimental Models: Organisms/Strains		
C57BL/6J *Ella*-Cre	Dr. David Ginsburg	N/A
C57BL/6J *Slx*$^{fl/fl}$	This manuscript	N/A
C57BL/6J *Slxl1*$^{fl/fl}$	This manuscript	N/A
CD1	Charles River Laboratories	Strain 022
C57BL/6J	Jackson Laboratory	Stock #000664
DBA2F1	Envigo	062
C57BL/6N	Envigo	044
Oligonucleotides		
Table S2	N/A	N/A
Software and Algorithms		
Kallisto	[33]	N/A
DESeq2	[34]	N/A
CRISPOR	[35]	N/A
Proteome Discoverer v2.1	Thermo Scientific	N/A
mrsFAST aligner	[36]	N/A
fastCN pipeline	[37]	N/A
Exalign	[38]	N/A
Dot-plots	Dr. David Page: https://pagelab.wi.mit.edu/materials-request.	N/A

LEAD CONTACT AND MATERIALS AVAILABILITY

Further information and requests for resources and reagents should be directed to and will be fulfilled by the Lead Contact, Jacob L. Mueller (jacobmu@umich.edu). The SLX/SLXL1, Rabbit polyclonal antibody we generated is available from our lab. Mice will be available from our lab until they become available from the Mutant Mouse Resource and Research Center Repository.

EXPERIMENTAL MODEL AND SUBJECT DETAILS

Transgenic mice used in this study were generated from injected zygotes (see Generation of transgenic lines) derived from the cross of F1 (DBA2xC57B/6N) and C57B/6N mice, ordered from Envigo. Heterozygous transgenic female mice were mated to C57BL/6J male mice ordered from Jackson Laboratory (Bar Harbor, ME) to backcross. Breeding was conducted with one male and one or two females, all mice were older than 6 weeks of age. Resulting pups were weaned at 21dpp, separated by sex and no more than 5 pups per cage (Allentown, 11.5in x 7.5in x 5in). All experiments were conducted with adult males (2-6 months of age) transgenic males were compared to wild-type littermates or age matched wild-type controls. Cages were kept on ventilated racks (Allentown) at 72°F, 30%–70% humidity, on 12hr: 12hr light:dark cycle. Cages are monitored daily and changed at least every two weeks in a room that is specific-pathogen free, monitored by sentinel mice. Mice were provided water and fed Lab Diet 5008 food *ad libitum.* Adult mice were sacrificed by CO_2 asphyxiation followed by cervical dislocation and pups were euthanized using decapitation in compliance with the ULAM standard procedures of euthanasia. The Institutional Animal Care and Use Committee at the University of Michigan Medical School (PRO00007498) approved all procedures involving mice.

METHOD DETAILS

Gene expression of mouse and rat X/Y co-amplified genes

RNA-seq analyses were conducted by analyzing previously published datasets. Specifically, mouse tissue panel data were analyzed from SRP016501 [39], fetal ovary data from SRP058992 [15], ovary data from SRP017959 [40], and sorted testicular germ cell populations from SRP113417 [14]. Rat tissue panel data was used from SRP016501 [39] and rat sorted testicular germ cell populations from SRP026340 [41]. Alignments were performed using Tophat with the mm10 mouse reference genome, a refFlat file with RefSeq gene annotations and max-multihits set to 240; otherwise standard default parameters were used. We used Cufflinks, using the refFlat RefSeq gene annotation file, to estimate expression levels as fragments per kilobase per millions of mapped fragments (FPKM).

Round spermatid FACS isolation and library generation

We largely followed a previously published protocol to isolate round spermatids (1n) [42]. Briefly, we disassociated cells from a pair of testes by enzymatic treatment with Collagenase type I (Worthington Biochemical Corporation), DNase I (Worthington Biochemical Corporation), and Trypsin (Life Technologies). The cell suspension was passed through cell strainers (100 μm and 40 μm) and incubated with Hoechst 33342 (Setareh Biotech) to determine DNA content and propidium iodide (Acros Organics) to evaluate cell viability. Cell sorting was performed on a Synergy Head Cell Sorter cell sorter (Sony). The purity of each sort was determined via fluorescence microscopy visual inspection of 100 cells morphology and nuclear staining with DAPI for round spermatids. The purity of round spermatids was typically > 85%, which is consistent with previous studies [42].

TRIzol LS (Thermo Fisher Scientific) was used to extract total RNA. RNA was DNase treated to remove any genomic DNA contamination using RNeasy Mini Kit and RNase-Free DNase Set (QIAGEN). Libraries were generated using samples with > 7 RIN scores and > 5ng of total RNA. Stranded mRNaseq libraries were generated using the NEBNext Ultra II Directional RNA Library Prep Kit (NEB) and Agencourt AMPure XP beads (Beckman Coulter) following the manufacturers protocol. We generated at least two biological replicate round spermatid mRNA-seq libraries per genotype. All libraries were sequenced on a single Illumina NovaSeq lane (~50 million sequenced fragments per library) and in NCBI SRA: PRJNA545829. Alignments were performed with Kallisto and DESeq2 using the RefSeq index with bootstrapping set to 100 [33, 34].

Generation of transgenic lines

To generate mice with multi-megabase deletions of the *Slx* and *Slxl1* ampliconic region, loxP sites were sequentially integrated upstream and downstream of either the *Slx* or *Slxl1* ampliconic region via CRISPR. sgRNA targeting unique sequence flanking the ampliconic region was selected based on scores from either the CRISPR Design Tool (http://www.genome-engineering.org/) or CRISPOR (http://crispor.tefor.net) [35]. sgRNA and Cas9 mRNA were synthesized *in vitro*, using the MEGAshorscript T7 kit (ThermoFisher) and mMESSAGE mMACHINE T7 ULTRA kit (ThermoFisher), respectively, followed by MEGAclear Kit (ThermoFisher) for clean-up. sgRNA, Cas9 mRNA, and single stranded oligo donor carrying the loxP sequence (IDT; Table S2) were mixed for microinjection at concentration of 50, 100, and 100 ng/ul, respectively. Cytoplasmic microinjection was performed on zygotes derived from the cross of F1 (DBA2xC57BL/6N) and C57BL/6N mice, using a piezo-driven microinjection technique [43]. Floxed mice were mated against C57B/6J *Ella*-Cre mice resulting in mice carrying either a *Slx* or *Slxl1* deletion or duplication (Figures 2B, 2C, 3A, and 3B). Two independent deletion and duplication lines were generated for each *Slx* and *Slxl1* ampliconic region. No differences were observed between independent lines and data was therefore compiled. All deletion or duplication carrying males were derived from heterozygous female mice that had been backcrossed to C57BL/6J males for at least four generations. Mice were genotyped by extracting DNA out of a tail biopsy using Viagen DirectPCR lysis reagent using primers that flank loxP sites (Table S2).

Testis Histology

Testes were collected from 2-6 months old mice. The tunica albuginea was nicked and the testes were fixed with Bouins Fixative overnight at 4°C. Testes were then washed through a series of ethanol washes (25%, 50%, 75% EtOH) before being stored in 75% EtOH at 25°C. Testes were paraffin embedded and 5μm sections were made that were stained with Periodic acid Schiff (PAS) and hematoxylin. Sections were studied using a light microscope and staged [44]. Specific types of germ cells were identified based upon their location, nuclear size and nuclear staining pattern [44].

Immunohistochemistry

Immunohistochemistry was performed on 5μm paraffin embedded sections. Sections were deparaffinized and rehydrated prior to antigen presentation. Antigen presentation was performed by boiling slides in 0.01M Citrate Buffer pH 6 for 10 minutes. Sections were blocked for 1hr at room temperature using 3% BSA and 0.05% Triton X-100 in PBS and subsequently probed with primary and secondary antibodies.

Our SLX/SLXL1 antibody was generated against a CVSFSEEWQRFARS-KLH conjugated peptide. Genemed Synthesis synthesized and injected the peptide into rabbits and affinity purified the antibody. Antibody specificity was assessed by probing whole testis lysates from wild-type (C57BL/6J), $Slx^{-/Y}$ and $Slxl1^{-/Y}$ mice with both pre-immune serum and purified antibodies on western blots. The following commercially available antibodies were used: SCP3 (Abcam, ab97672), Peroxidase AffiniPure (Jackson ImmunoResearch, 711-035-152), FITC AffiniPure (Jackson ImmunoResearch, 711-095-152), Rhodamine RedX AffiniPure (Jackson ImmunoResearch, 715-295-151).

RT-PCR

Total RNA was extracted using Trizol (Life Technologies) according to manufacturer's instructions. Ten μg of total RNA was DNase treated using Turbo DNase (Life Technologies) and reverse transcribed using Superscript II (Invitrogen) using oligo(dT) primers following manufactures instructions. Intron-spanning primers were used to perform RT-PCR on adult testis cDNA preparations for *Slx, Slxl1* and a round spermatid specific gene *Trim42* (Table S2).

Assaying Fertility

The fecundity of males was assessed by mating at least three males 2-6 months of age of a given genotype to 2-6 month old C57B/6J females and monitoring females for copulatory plugs. The fertility of all lines was compared to that of C57B/6J males (wild-type). Offspring sex ratios data was compiled by sex genotyping offspring from the aforementioned crosses as well as pups resulting from males bred with CD1 females. Sperm counts were conducted on sperm isolated from the cauda epididymis. Briefly, the cauda epididymis was isolated and nicked three times to allow sperm to swim out. The nicked epididymis was then rotated for 1hr at 37°C in Toyoda Yokoyama Hosi media (TYH). Sperm were fixed in 4% PFA and counted using a hemocytometer. For each genotype, at least three male mice were counted with three technical replicates performed for each mouse and averaged. Testes were collected from 2-6 month old males for all experiments and weighed, along with total body, in order to determine relative testis weight.

X-Y Chromosome Paint

Cauda epididymal sperm were collected and fixed onto slides using 3:1 methanol: acetic acid. Slides were stored at −20°C. Slides were immersed twice in 2x SSC for three minutes followed by a series of ethanol washes (70%, 90%, 100% ethanol) for two minutes each. Slides were incubated at room temperature for 30 minutes in 5mM DTT, 1% Triton X-100, 50mM Tris. Slides were again washed with 2x SSC and the ethanol series. Slides were incubated in 70% formamide, 2x SSC at 78°C for five minutes and then washed in ethanol series for one minute each. Mouse X and Y paint probes from MetaSystems Probes were mixed and denatured at 80°C for ten minutes before placing on slide. Slides were incubated overnight at 37°C in a humid chamber. Slides were washed in 50% formamide, 2x SSC three times at 45°C for five minutes, 2x SSC once at 45°C for five minutes and rinsed in Photo-Flo 200 (Kodak). Slides were mounted with VECTASHIELD with DAPI (Vector Laboratories).

Co-Immunoprecipitation and Mass Spectrometry

SLX/SLXL1 co-immunoprecipitation was performed on whole testis lysate using our SLX/SLXL1 antibody conjugated to protein A Dynabeads (Life Technologies). Briefly, testes from wild-type, $Slx^{-/Y}$, $Slxl1^{-/Y}$ and $Slx^{-/Y}$, $Slxl1^{-/Y}$ males were lysed (150 mM KCl, 0.05% NP-40, 0.5 mM DTT, and protease inhibitors (EDTA-free Complete PI)) and centrifuged at full speed in a tabletop centrifuge at 4°C. The top lipid layer was discarded and the remaining supernatant was transferred to a new tube and incubated with SLX/SLXL1 antibody. Protein A dynabeads were rinsed 3 times with lysis buffer before adding the lysate/antibody solution and incubated at 4°C for at least 1hr. Beads were subsequently washed 2X with lysis buffer and 1X with lysis buffer containing no detergent and 1X with PBS containing protease inhibitors. A small aliquot of beads was removed for western blot analysis. The remaining beads were stored at −20°C after removing all liquid. Prior to trypsin digestion, beads were resuspended in 50ul of 0.1M ammonium bicarbonate buffer (pH∼8). Cysteines were reduced by adding 50ul of 10 mM DTT and incubated at 45°C for 30 min. To alkylate cysteines, the samples incubated at room temperature, protected from light, with 65 mM 2-Chloroacetamide. Proteins were digested overnight with 1μg sequencing grade modified trypsin at 37°C with constant shaking in a Thermomixer. Digestion was stopped by acidification and peptides were desalted using SepPak C18 cartridges using manufacturer's protocol (Waters). Samples were dried using a vacufuge. Samples were dissolved in 8μl of 0.1% formic acid, 2% acetonitrile solution and then 2μl of the peptide solution was resolved on a nano-capillary reverse phase column (Acclaim PepMap C18, 2 micron, 50 cm, ThermoScientific) using a 0.1% formic acid, 2% acetonitrile (Buffer A) and 0.1% formic acid, 95% acetonitrile (Buffer B) gradient at 300 nl/min over a period of 180 min (2%–22% buffer B in 110 min, 22%–40% in 25 min, 40%–90% in 5 min followed by holding at 90% buffer B for 5 min and requilibration with Buffer A for 25 min). Eluent was directly introduced into Orbitrap Fusion tribrid mass spectrometer (Thermo Scientific, San Jose CA) using an EasySpray source. MS1 scans were acquired at 120K resolution (AGC target = $1x10^6$; max IT = 50 ms). Data-dependent collision induced dissociation MS/MS spectra were acquired using Top speed method (3 s) following each MS1 scan (NCE ∼32%; AGC target $1x10^5$; max IT 45 ms).

Proteins were identified by searching the MS/MS data against *Mus musculus* (UniProt; 60627 entries) using Proteome Discoverer (v2.1, Thermo Scientific). Search parameters included MS1 mass tolerance of 10 ppm and fragment tolerance of 0.2 Da; two missed cleavages were allowed; carbamidimethylation of cysteine was considered fixed modification and oxidation of methionine, deamidation of aspergine and glutamine were considered as potential modifications. False discovery rate (FDR) was determined using Percolator and proteins/peptides with a FDR of ≤ 1% were retained for further analysis.

Candidate interacting proteins were filtered based upon high confidence (< 1% FDR), reproducible presence across multiple wild-type samples (PSM > 5) and reproducible absence across all $Slx^{-/Y}$, $Slxl1^{-/Y}$ samples. Three biological replicates-wild-type and $Slx^{-/Y}$, $Slxl1^{-/Y}$, two biological replicates $Slx^{-/Y}$ and $Slxl1^{-/Y}$ were performed. The mass spectrometry proteomics data have been deposited to the ProteomeXchange Consortium via the PRIDE [45] partner repository with the dataset identifier PXD014276.

Estimation of amplicon copy number

For estimating the number of *Slxl1* copies in the rat genome, read depth analysis was performed using the mrsFAST [36] aligner and the fastCN pipeline [37]. Reads were mapped against the rn6 reference genome in which sequences identified by RepeatMasker, Tandom Repeat Finder, and 50-mers with an occurrence greater than 50 were masked. Read depth was normalized to account for GC content, averaged in windows containing 3,000 unmasked positions, and converted to copy-number based on the observed depth in autosomal regions not previously identified as copy-number variable [46]. Analysis was performed using male and female genomic data obtained from SRP029216 [47].

Comparisons of exon-intron structure

Complete RefSeq mRNA sequences were obtained for mouse *Sycp3* (NM_011517), *Slx* (NM_001136476), *Slxl1* (NM_029181), and *Sly* (NM_201530). Pairwise comparisons for each of the four genes were performed via Exalign [38] to determine conservation on exon-intron structure.

Dot-plots

Self-symmetry triangular dot plots that show repeats within a sequenced region were generated from a custom Perl script that can be found at https://pagelab.wi.mit.edu/materials-request.

Round spermatid Injections (ROSI)

Round spermatids were collected and enriched from the testes of 2-6 month old WT and *Slx* $^{-/Y}$,*Slxl1* $^{-/Y}$ males, as described previously [48]. Briefly, testes were placed in red blood cell lysis solution (Miltenyi Biotec) to remove Tunica albuginea. Seminiferous tubules were transferred to GL-PBS (0.01% PVP in Dulbecco's PBS containing glucose and pyruvate from GIBCO), cut into small pieces and pipetted gently to release spermatogenic cells. The cell suspension was filtered through a 50-um nylon mesh, centrifuged at 200xg for 5 min at 4°C, and resuspended in GL-PBS containing 0.4 mg/ml pronase E (SERVA). The cell suspension was centrifuged again at 400xg for 5 min at 4°C to precipitate most elongating spermatids and spermatozoa. The remaining suspension containing most round spermatids was washed twice at 200xg for 5 min at 4°C and stored in 7.5% glycerol, 7.5% FBS, 0.01% PVP in GL-PBS at −80°C.

Unfertilized eggs were harvested from 5-weeks-old superovulated C57BL6/DBA2 F1 females. Round spermatids were thawed and washed twice with 7.5% FBS in GL-PBS at 400xg for 5 min at 4°C. More than 90% cells were alive after thawing, as determined by the trypan blue extrusion test. On the injection dish, eggs and round spermatids were placed in a droplet of the M2 medium (Sigma) and a droplet of GL-PBS, respectively. Using a needle with 6um inner diameter and 15 um outer diameter for piezo-driven microinjection, individual round spermatids were drawn into the needle to break the plasma membrane, and the nucleus was injected into the cytoplasm of the egg. Following round spermatid injection, eggs were activated in the M16 medium (Sigma) containing 5 mM $SrCl_2$ and 5 mM EGTA for 20 min at 37°C [49]. Eggs were then washed and cultured in KSOM media for development.

QUANTIFICATION AND STATISTICAL ANALYSIS

Two-tailed Fisher's Exact tests were used to calculate statistical significance between wild-type and transgenic groups in offspring sex ratio (Figure 3) and X versus Y sperm counts (Figure 3) as the outcomes are binary. The number of pups or sperm screened are noted in the figure and figure legend, respectively. To determine statistical significance for average litter size, sperm counts and testis weights between wild-type and transgenic groups, a two-tailed t test was performed. The number of mice used is denoted in the figure legends. All error bars denote standard deviation.

DATA AND CODE AVAILABILITY

Sequencing data is available on NCBI SRA: PRJNA545829. Mass spectrometry data is available on the PRIDE database: PXD014276.